EBSD Evaluation of Al- TiAl₃ Composites Manufactured Through CRB-Annealing-ARB and CRB-ARB-Annealing Methods

Zohreh Yazdani[1] · Mohammad Reza Toroghinejad[1] · Hossein Edris[1]

Abstract In this study, Al-TiAl₃ nanocomposites were produced by applying annealing treatment (AT) before and after the accumulative roll bonding (ARB). First, the sandwich of two Al sheets containing pure Ti powder was subjected to cold roll bonding (CRB) and then underwent AT-ARB and ARB-AT processes. Annealing conditions were used to form the intermetallic compound at 590 °C for 2 h, and the ARB process was performed for a maximum of five cycles. The chemical and microstructural revolutions were evaluated using field emission scanning electron microscopy (FESEM) equipped with an elemental analyzer (EDS) and electron backscatter diffraction (EBSD) analysis. The results showed that through annealing after CRB, TiAl₃ intermetallic compound was formed in the Al matrix, and then, the obtained Al-TiAl₃ composite was subjected to the ARB process. Finally, a composite containing a uniform distribution of TiAl₃ particles of larger than 200 nm in the Al matrix was obtained. Microstructural changes showed that with an increase in strain due to the development of continuous recrystallization, a structure containing grains smaller than 500 nm was obtained. The microstructural evaluation of the ARB-AT composite showed that the grain size of Al and particle size of TiAl₃, in this case, were in micrometer and larger.

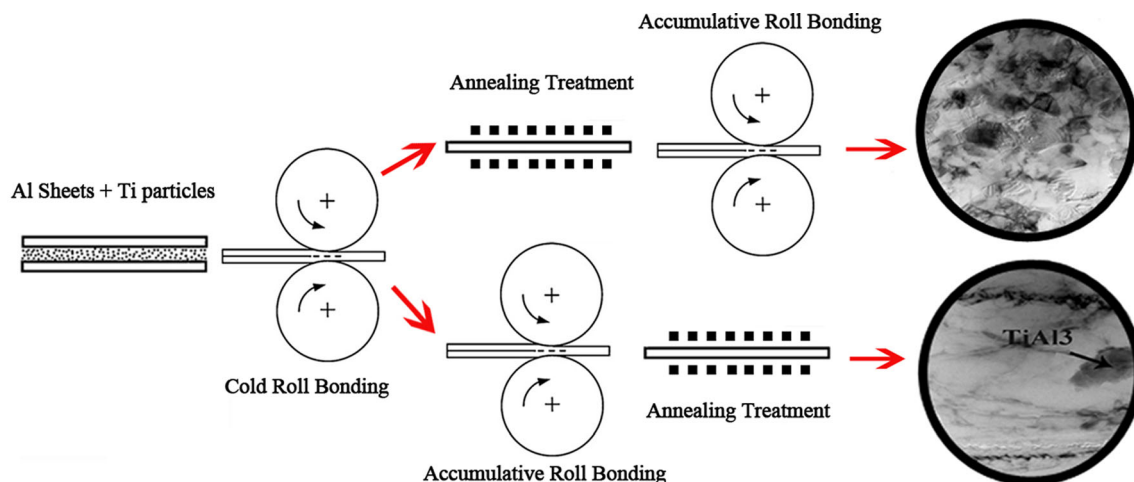Mohammad Reza Toroghinejad and Hossein Edris are Co-authors.

✉ Zohreh Yazdani
  z.yazdani@alumni.iut.ac.ir

  Mohammad Reza Toroghinejad
  toroghi@cc.iut.ac.ir

  Hossein Edris
  h-edris@cc.iut.ac.ir

[1] Department of Materials Engineering, Isfahan University of Technology, 84156-83111 Isfahan, Iran

Graphic Abstract

Keywords ARB · Ti aluminide · Metal matrix composite · EBSD · Intermetallic compounds · $TiAl_3$

1 Introduction

Recently, much interest has been directed toward Al metal matrix composites due to their lightweight, high elastic modulus, and suitable electrical and magnetic properties. They have many modern and advanced applications in the aerospace, defense, and automotive industries [1]. Particle reinforcements in Al matrix composites are mainly ceramic particles such as SiC and Al_2O_3. Ceramic reinforcements have a comparatively low density (about 3 g/cm^3) and a superior elastic modulus (200–200 GPa) [2]. Metal aluminides are intermetallic compounds with a density near to that of ceramics; in addition, some of them have an elastic modulus comparable to that of ceramics. Most significantly, they are in thermodynamic equilibrium with the Al matrix. Therefore, there is an actual chemical bond between Al and its reinforcing aluminides. In ceramics, there is only one intermediate reaction zone.

Among the aluminides, Ti aluminide, in addition to having these specifications, is one of the compounds with the highest elastic modulus and melting point. The composite comprises of Ti aluminides, and thus, a combination of low density, high strength of Ti aluminides, and good toughness of Al; moreover, it maintains the desired high temperature of aluminides [3, 4]. $TiAl_3$ intermetallic compound, as the most thermodynamically stable intermetallic composition of the Ti–Al diagram, has an enthalpy

of − 34 kcal/mol and Gibbs free energy of − 32.5 kcal/mol [5].

Common fabrication methods for particle-reinforced metal-based composites include powder metallurgy, casting, and spray deposition. Due to the high cost of the equipment required and the complicated procedure of the production methods, the expense of fabricating metal-based composites through these procedures is significant, which has restricted the uses of these materials. Among the conventional composite fabrication techniques, the cold roll bonding (CRB) and annealing process have experienced rapid growth in the last decade because of their high performance and cost-effectiveness compared to the other methods. The solid-state roll welding process, which involves an atom–atom bond between two layers, has been widely used to bond the same and different types of metals through rolling in the manufacturing of foil and multilayer composite sheets.

Past research has shown that materials with nanometer grain size exhibit unique characteristics such as high strength, super plasticity at high strain rates and low temperatures, and excellent corrosion resistance. Severe plastic deformation methods with high plastic strain are extensively applied to fabricate nanograin substances. One of these methods of making fine-grained sheets is the accumulative roll bonding (ARB) process. In this process, strain is distributed almost uniformly throughout the grains. Due to the repetition of the process, metal or intermetallic reinforcing particles that may exist between layers can uniformly distribute in the matrix.

ARB method may also be considered as a method of mass production of sheets with this property [6–8]. In this

process, two sheets with a thickness of t are placed over each other and then rolled. The rolling process must be such that the thickness of the two sheets on top of each other (t_2) is equal to the thickness t (i.e., the deformation rate is equal to 50%). The two-layer sheet, which is now of thickness, is cut into half, and then, one side of each half is roughened and they are stacked on top of each other. They are then rolled again, as mentioned. Repeating this process causes a relatively high deformation in each layer during each cycle, thus causing severe plastic deformation throughout the sheet.

In the ARB process, the application of severe plastic deformation to multilayer materials and fine-graining leads to incidental dislocation boundaries and necessary geometric boundaries [6]. Moreover, the cold rolling process, by producing dislocations and other crystal defects, accelerates the reactions during the subsequent diffusion operation and speeds up the formation of the intermetallic Ti aluminide compound through annealing. Therefore, by using the CRB process on Al–Ti and then annealing, an Al-based composite with aluminide compounds can be obtained [4].

Previous researches have mainly involved rolling or ARB and then annealing to make reinforcing particles. Through this process, it is impossible to reach a final product with a small grain size and good mechanical properties [9–13]. Nevertheless, there is little research on performing ARB on composite samples obtained in primary roll bonding and annealing to achieve uniform particle distribution. For example, Liu et al. [14] obtained an Al-based composite with Al_3Mg_2 reinforcement particles through hot roll bonding, vacuum annealing, and, finally, ARB of Al sheets and Mg foil. However, the implementation of, first, roll bonding and annealing and then ARB on the composite to distribute the reinforcing particles and to obtain a fine-grain structure was proposed by Yazdani et al. [15] as a new method for Al sheet/Ti powder/Al sheet layers. In their previous work, they successfully implemented this method in the Al-Ti system and reached a nanocomposite with a strength of 400 MPa. First, CRB and annealing processes led to the development of intermetallic particles. Then, ARB led to the achievement of a composite with a homogeneous distribution of intermetallic compounds with nanoparticle size in the Al matrix. In this research, Al-based composites with Ti aluminide reinforcements were also fabricated and evaluated through CRB, annealing and then ARB in order to compare the results with the results of the common method applied by others [10, 16]. For the first time, a more detailed study of microstructural changes was performed using the electron backscatter diffraction (EBSD) test on two composites, and the effect of annealing before and after ARB was determined to obtain more comprehensive information about this new fabrication method.

2 Materials and Methods

For the fabrication of Al/Ti aluminide composite, 1100 Al sheets (with 99.5 wt. % of Al) with dimensions of $100 \times 50 \times 100$ mm were used. The annealing process was applied to these sheets at 350 °C for 1 h to remove the rolling history in the material. Consumable Ti powder with 99% purity and an average size of 0.8 µm was prepared by Merck & Co. (Kenilworth, NJ, USA). Annealed Al sheets were cut to 100×50 mm². After washing them with acid and cleaning them with acetone, they were brushed. A wire brush with an outer diameter of 6 cm was selected for brushing. To apply Ti powder between the Al sheets, the powders were poured into ethanol solution and then sprayed only on the surface of one sheet. To prevent re-contamination of the surfaces, the rolling process must be performed within 120 s after surface preparation. Finally, the rolling process was performed using a rolling machine with a rotation speed of 10 rpm. Annealing of the samples was performed in an electric furnace. To protect the samples from oxidation, the samples were placed in containers containing alumina powders. Subsequently, the samples were heated to the determined temperatures at a heating rate of 10 °C/min and then were cooled in the furnace. The samples were then subjected to the ARB process for a maximum of five cycles. To prevent the spread of edge cracks created during ARB cycles, the cracked parts were cut after each cycle. The temperature conditions selected according to a previous work of the authors of the present study [15] were 590 °C for 2 h; the percentage of deformation implemented was determined according to another research by these authors [17]. Al sheet sandwiches with 0.5wt% of Ti (0.2 g of Ti powder) added between them were subjected to CRB with 50% deformation (CRB sample). For the formation of the intermetallic compound at the interface between the sheets, after CRB, annealing treatment was performed (CRB-AT sample). The ARB process was then applied to these samples for a maximum of five cycles. These samples were named CRB-AT-ARB. Al samples without reinforcing particles were produced under the same manufacturing conditions and were called Al-ARB.

For comparison, some 1100 Al sheet sandwich samples containing 0.5wt% of Ti powder, after CRB without intermediate annealing, underwent ARB process for a maximum of five cycles (CRB-ARB sample), and, finally, for the formation of the intermetallic compound, they were annealed and named CRB-ARB-AT. In these samples, the intermediate annealing stage was eliminated, and the

formation of intermetallic composition due to annealing occurred after ARB.

To calculate the parameters required for determining the dislocation densities, X-ray diffraction (XRD) evaluation was used. XRD tests were carried out using a diffractometer (model X'pert MPD; Philips, Amsterdam, Netherlands) at a current of 30 mA and a voltage of 40 kV. A field emission scanning electron (FESEM) microscope (model S-4800; Hitachi, Chiyoda City, Tokyo, Japan) was employed to evaluate the microstructure and particle distributions of the obtained phase. The microscope was also equipped with an elemental analyzer for energy-dispersive X-ray spectroscopy (EDS) to achieve elemental analysis and element distribution maps. Uniaxial tensile tests were employed to evaluate the tensile behavior of the samples. Tensile strength samples were prepared alongside the rolling direction, and the tests were done at a rate of 1 mm/min. The sub-surface areas of the samples were prepared for SEM evaluation using focused ion milling (FIB) in SEM (Quanta 200-3D; FEI Company, USA) using a current of 20 nA to a depth of 1 μm. A FESEM microscope (LEO 1530 FEG, ZEISS, Jena, Germany) was used to investigate the orientation of the grains. This analysis was performed at a voltage of 20 kV on the RD-ND plane at exactly half the thickness. The used step size was determined in the range of 0.05–2 μm, according to sample type. According to the agreement, high-angle grain boundaries were defined as grain boundaries with a misorientation degree of above 15°. Low-angle grain boundaries were defined as grain boundaries with a misorientation degree between 2° and 15°. The data obtained from the EBSD analysis detector were processed using MTEX software. To obtain the geometric characteristics of powder particles, including size, shape, and particle distribution, and to calculate the percentage of phases, digital image processing software was used.

Equivalent strain or ε_{eq} after n cycles of the ARB is demonstrated as Eq. 1 [18].

$$\varepsilon_{eq} = \frac{\sqrt{3}}{2}\ln(r), \quad r = 1 - \frac{t}{t_0} = 1 - \frac{1}{2^n} \qquad (1)$$

where t_0 is the initial thickness of the layers that are placed on top of each other, r is the thickness reduction for each cycle, and t is the thickness after rolling. For ARB with 50% thickness reduction for each cycle, $|\varepsilon_{eq}|$ is equal to 0.8 n.

XRD test was utilized to measure the sub-grain size (crystallite size) and the amount of micro-strain applied to the samples. The Rietveld refinement method was employed to inspect the X-ray diffraction patterns. To measure the mentioned parameters, the XRD patterns of samples were analyzed in MAUD software. In the present study, the diffraction patterns obtained from the X-ray

diffraction test using MAUD software were matched to the graph calculated by the software so that the goodness-of-fit (GOF) was always less than 2. This factor shows the degree of conformity of the laboratory diffraction patterns with the computational graphs. Dislocation densities can be obtained indirectly through the Rietveld method and with the help of microstructural analysis results. Using the method proposed by Smallman-Westmacott [19], the dislocation densities (ρ) can be obtained from the values of micro-strain (ε) and crystallite size (D) in the form of Eq. (2):

$$\rho = (\rho_D \rho_S)^{1/2} \qquad (2)$$

where ρ_D is the dislocation density due to the size of the crystallite and ρ_S is the dislocation density due to the micro-crack, and these are calculated using the following equations:

$$\rho_D = \frac{3}{D^2} \qquad (3)$$

$$\rho_S = \frac{6\pi(\varepsilon^2)}{b^2} \qquad (4)$$

In the above relation, b is the Burgers vector, and its value for the face-centered cubic (FCC) lattice is equal to $\frac{a}{\sqrt{2}}$ (a represents the lattice parameter). In summary, the density of dislocations can be obtained using Eq. 5.

$$\rho = \frac{3\sqrt{2\pi}(\varepsilon^2)^{1/2}}{Db} \qquad (5)$$

3 Results and Discussion

3.1 Microstructural Evaluations in CRB-AT-ARB and CRB-ARB-AT Samples

3.1.1 CRB-AT-ARB Composite

For the first group of specimens, after the initial CRB of Al sheet/Ti powder/Al sheet, annealing is performed. Performing annealing for these powder specifications results in the complete conversion of Ti and $TiAl_3$ intermetallic composite particles formed throughout the interface. In the Ti and Al diffusion couple, it has been observed that in most cases, the $TiAl_3$ phase is the first phase to be formed and is also the phase that is created in large quantities at temperatures under the Al melting point. It is suggested that this is due to the increase in the number of unoccupied spaces in the Al lattice in the $TiAl_3$ layer. They speculated that in the presence of such a gradient, Al diffuses more rapidly, preventing the formation and growth of any expected intermediate phase [20, 21]. Formation mechanism of $TiAl_3$ intermetallic in a Al-Ti system during heat treatment can be described by increasing of Ti and $TiAl_3$

Fig. 1 (**a**) and (**b**) SEM images of the distribution of TiAl$_3$ intermetallic composite particles in the CRB-AT-ARB5 sample and (**c**) and (**d**) Relevant EDS analysis of one of the particles in this sample
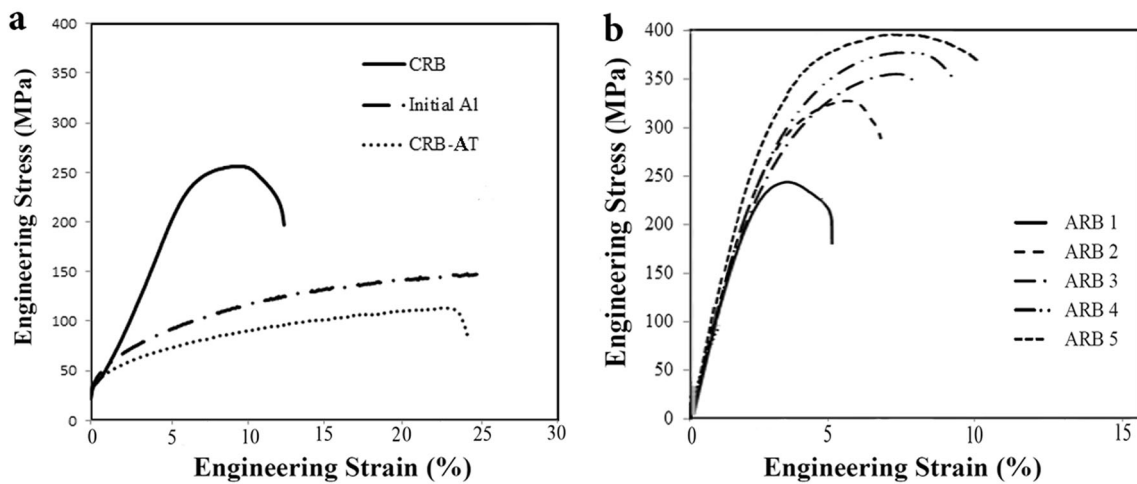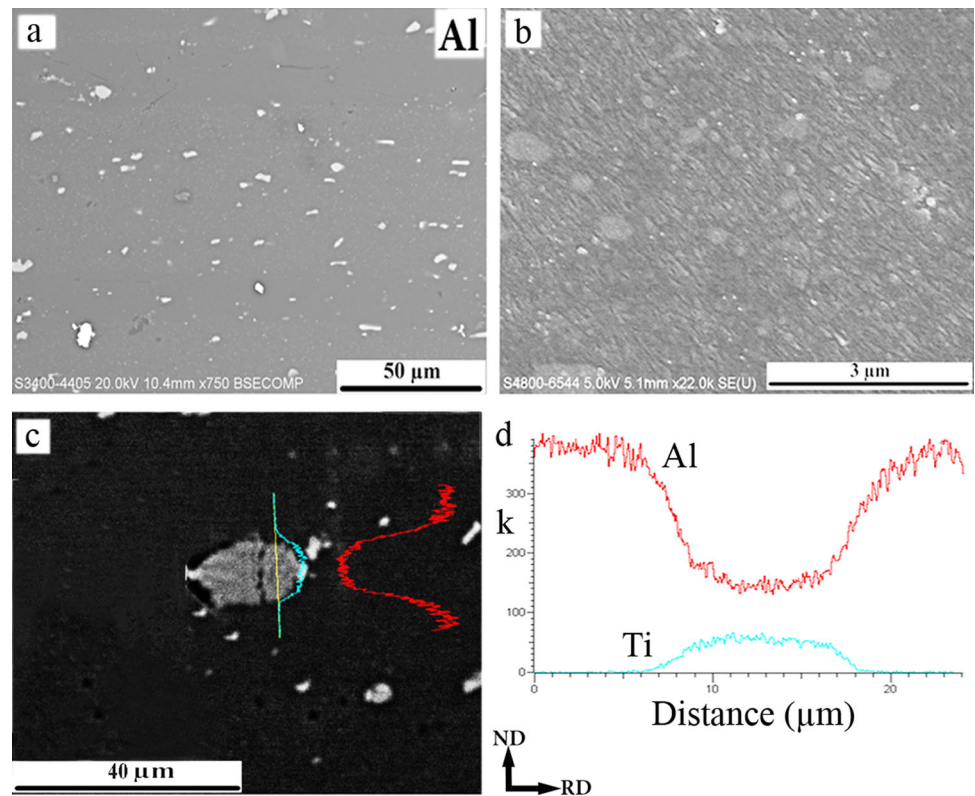
Fig. 2 Engineering stress–strain curves of **a** initial Al, CRB, and CRB-AT, and **b** CRB-AT-ARB samples after 1 to 5 ARB cycles

phase masses, formation of micro-cracks, higher diffusion of Al in Ti and remaining Kirkendall voids in Al, volume increase at Ti and TiAl$_3$ phases, micro-cracks established along with particles and easier formation of brittle TiAl$_3$ [22]. The dislocation density is calculated using Eq. 5. The results show that in the CRB sample, the dislocation density is equal to 7×10^{13} m^{-2}. After annealing, the dislocation density decreases to 3.6×10^{13} m^{-2}.

In obtained Al–TiAl$_3$ composite, the intermetallic particles are still located in the previous locations of the Ti through the interface of the two Al sheets. Therefore, the primary aim of applying the ARB technique in the next step is the breakup of intermetallic particles and their uniform distribution in the Al matrix. Furthermore, continuous plastic deformation in the ARB method can assist the removal of Kirkendall voids caused by the formation of intermetallic compounds and thus enhance the mechanical

properties of the composite. Figure 1a and b shows microscopic pictures of the CRB-AT-ARB composite made in the fifth ARB cycle (with a strain of 4). As can be seen, with ARB, the intermetallic composite particles break up due to the vertical compressive force of the roller and the increase in the length of the rolled sheets, and a better dispersion is seen in the particles. Moreover, the microstructure has an acceptable distribution of particles with a maximum size of 5 μm. In addition, Kirkendall voids are not visible at this scale. The reduction in voids improves the bonding quality between intermetallic particles and the bonding quality between the two Al sheets and, ultimately, enhances the strength of the composite [23]. According to the previous work of these authors [15], the tensile strength of this composite after the fifth cycle gets to 400 MPa, which is remarkably higher than the 300 MPa of monolithic Al prepared in the same way.

The results of elemental analysis of one of the particles in this composite (Fig. 1c) are shown in Fig. 1d. This indicates that no phase change has occurred during ARB, and finally, an Al matrix composite with $TiAl_3$ intermetallic reinforcement particles is obtained. It is known that with an increase in the number of cycles of the ARB process, the number of layers increases. This increase in the number of layers increases the homogeneity of the intermetallic particle distribution in the ND direction. Another reason for particle uniformity with growing ARB cycles may be the effect of friction in the middle of the roller and the sheet. Initially, a sharp plastic deformation occurs below the surface and is transferred to the middle of the sandwich with the repetition of the ARB process. The calculated dislocation density for this sample is 45×10^{13} m^{-2}.

The engineering stress–strain curves of CRB-AT-ARB composite samples are shown in Fig. 2. The initial Al sample had an ultimate tensile strength of 150 MPa (according to Fig. 2a). After cold roll bonding, its ultimate strength increases to 250 MPa, while its ductility decreases. In the CRB-AT sample, the ductility decreases

however, its value is still less than that of the initial Al sample. Figure 2b shows the stress–strain curves of the CRB-AT-ARB samples in different ARB cycles. As demonstrated, after the first cycle of the ARB, ductility decreases in comparison with the CRB-AT sample, and strength increases to 240 MPa. Subsequent cycles of the ARB lead to the gradual improvement of ductility and strength, with the final strength after five ARB cycles reaching 400 MPa, a great value for an Al alloy. The elongation of the CRB-AT sample is 23%, which decreases by 4% after the first cycle of the ARB procedure. The ductility is gradually enhanced by increasing the number of ARB cycles. Eventually, the ductility of the composite with $TiAl_3$ particles after five cycles of the ARB is 10%. $TiAl_3$ in the CRB-AT-ARB5 sample is uniformly distributed in the Al matrix with an ultra-fine grain structure (Fig. 1a). Therefore, the composite containing Ti aluminide has higher strength than the Al sample produced using the same method without Ti powder, which has an ultimate tensile strength of 300 MPa [15, 24]. The increase in strength by raising ARB cycles can be due to increased deformation, decreased grain size, enhanced dislocation density, and the pinning of the grain boundaries by hard intermetallic particles [25]. In the other word, the presence of particles affects the mean dislocation activity significantly [26].

When the intermetallic compound is formed during annealing at 590 °C for 2 h, the Kirkendall pores are produced. In these composites, an increase in ductility by growing the ARB cycles after annealing can be related to the removal of Kirkendall pores due to the subsequent ARB rolling. This can be seen in the SEM images of the longitudinal cross sections of the samples (normal to the TD) prepared through Focused Ion Beam (FIB) milling (Fig. 3). The SEM images after one (Fig. 3a) and five (Fig. 3b) ARB cycles indicate a reduction in the number and size of the pores by extending ARB cycles. Moreover, Fig. 3a displays a discontinuity in the interface of Al layers; after five cycles of ARB (Fig. 3b), the number of these

Fig. 3 SEM images of **a** CRB-AT-ARB1, (Al layers' interface discontinuities are shown with black arrows), and **b** ARB-AT-ARB5 samples after FIB milling
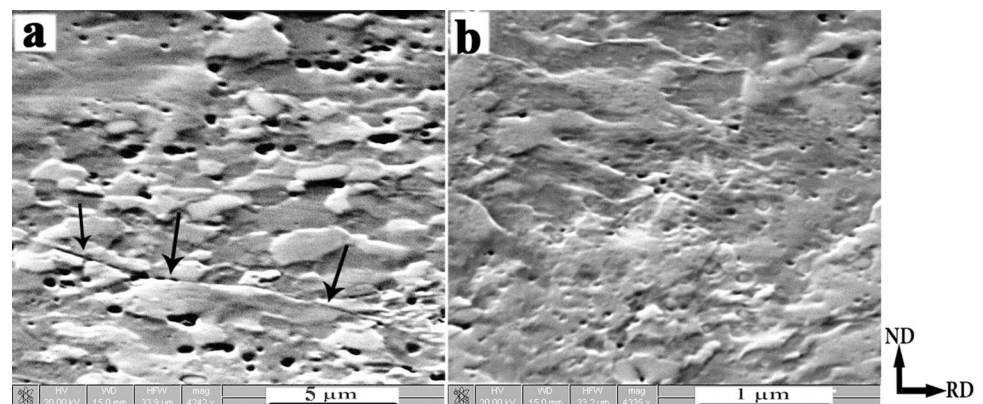
Fig. 4 (a) and (b) SEM images of the distribution of TiAl$_3$ intermetallic particles in the CRB-ARB5-AT sample and (c) and (d) Relevant EDS analysis of one of the particles in this sample
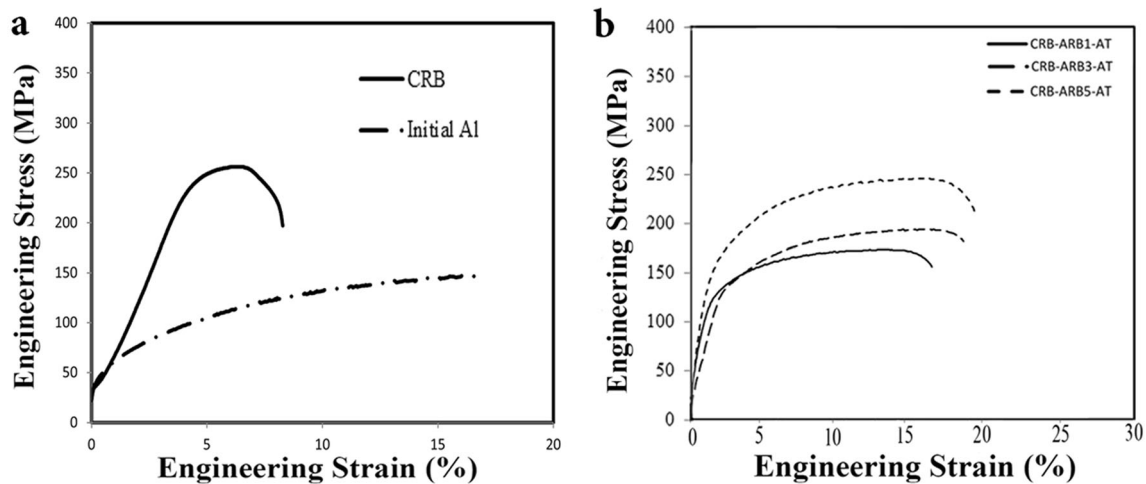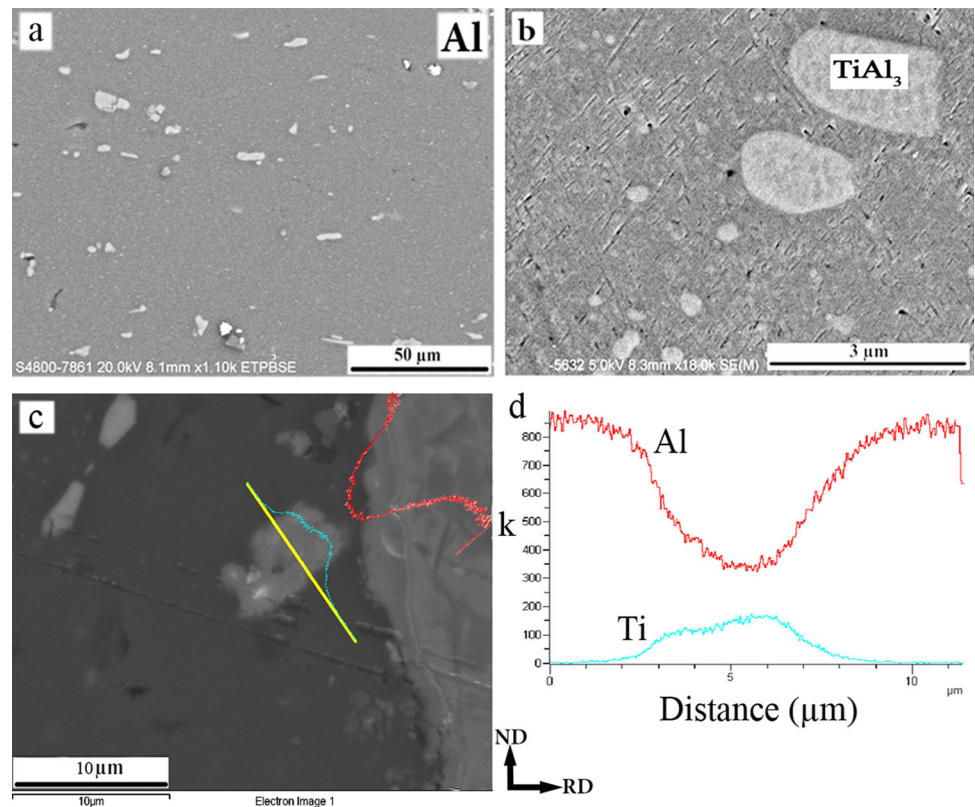

Fig. 5 Engineering stress–strain curves of a initial Al and CRB and b CRB-ARB1-AT, CRB-ARB3-AT, and CRB-ARB5-AT samples

discontinuities is significantly smaller. This shows better bonding between the layers, as well as at the matrix–reinforcement phase interface, which can be an ineffective factor in decreasing porosity.

3.1.2 CRB-ARB-AT Composite

In the second fabrication method, Al /Ti powder/Al is roll bonded and then undergoes five cycles of ARB procedure and, finally, is annealed. Figure 4 displays the annealing

results for the CRB-ARB sample that underwent five ARB cycles. According to Fig. 4a and b, the particle size of the intermetallic compound has decreased due to the increase in the number of ARB cycles. However, due to the presence of large Ti particles after five ARB cycles, the TiAl$_3$ intermetallic compound is present in different sizes in the microstructure. According to these images, after five cycles of ARB and annealing, fine intermetallic particles as small as 200 nm are present in the microstructure along with large micrometer particles. Moreover, the morphology of
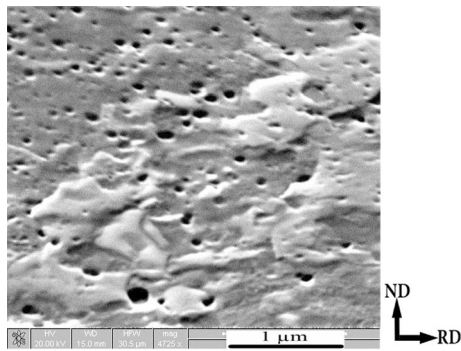
Fig. 6 SEM images of CRB-ARB5-AT sample after FIB milling

the smaller particles is very close to spherical. The elemental analysis results are demonstrated in Fig. 4c and d, which show the formation of the $TiAl_3$ intermetallic compound in the Al matrix. It is clear that after annealing, the amount of defects, including the density of dislocations, decreases. Calculation of dislocation densities show that this factor is 0.05×10^{13} m^{-2} in the CRB-ARB1-AT sample, 0.22×10^{13} m^{-2} in the CRB-ARB3-AT sample and reduces to 0.8×10^{13} m^{-2} in the CRB-ARB5-AT sample. The researchers suggested that in the Al/Ti diffusion system, the Al element diffuses more easily into the Ti. Therefore, Al is the only diffusion element in the diffusion coupling of this system. Al has a much higher diffusion rate than Ti. Moreover, the diffusion of Ti atoms toward Al is much higher than the diffusion of Al into Ti. As soon as the $TiAl_3$ intermetallic layer is formed, Ti is limited to diffusion through $TiAl_3$ and, therefore, will not be able to diffuse through and inside Al, but Al is free to diffuse into $TiAl_3$ and Ti [27].

Figure 5 shows the engineering stress–strain curves of the CRB-ARB-AT samples. Figure 5a, similar to Fig. 2a, shows that CRB has increased the strength and decreased the ductility of the sample compared to the initial Al. Figure 5b shows that the strength of the sample that has undergone one cycle of the ARB procedure before annealing is 160 MPa. By growing ARB cycles, the strength of the samples is expanded, and the ultimate tensile strength of CRB-ARB5-AT is 240 MPa. Ductility also increases from 17% after one cycle to 20% after five cycles. The initial Al has an elongation of 24% and ultimate tensile strength of 150 MPa, is observed in Fig. 2a. Although annealing at 590 °C for 2 h after five cycles of ARB process has increased the ductility, the results show that annealing as the last step of the process has derived a reduction in strength. The strength of this sample (240 MPa) is not significantly greater than that of the initial Al and is substantially lower than the 400 MPa of the CRB-AT-ARB5 sample (Fig. 2b). Revolutions in strength and microstructure are fully consistent with each other. It can be seen that as a result of annealing after the ARB procedure, the structure undergoes a recovery process resulting in decreased dislocation density, as well as recrystallization, and, finally, grain growth. This process decreases strength while improving ductility. In addition, the driving force of recrystallization is the energy stored as a result of cold work. This means that the extent of recrystallization increases with an increase in cold work, turning sub-grain boundaries into main grain boundaries.

The SEM image of the CRB-ARB5-AT sample after FIB milling indicated in Fig. 6 demonstrates a high density of Kirkendall pores and their distribution in the microstructure. In these specimens, because of the

Fig. 7 XRD patterns of **a** Initial Al, **b** CRB, **c** CRB-AT, **d** CRB-AT-ARB5 and **e** CRB-ARB5-AT samples
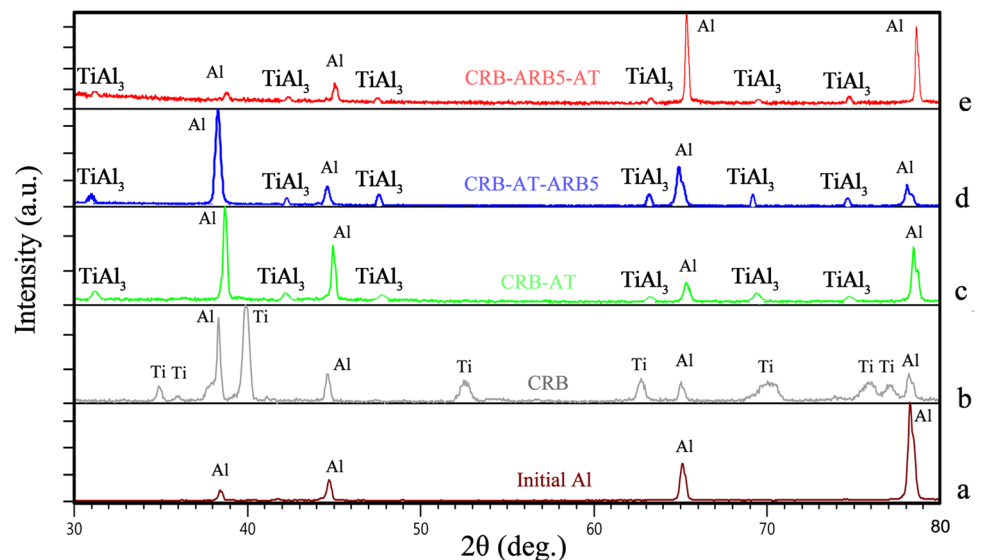
Fig. 8 Images obtained from the EBSD analysis of the CRB-AT sample in the ND-RD section, including **a** electron image, **b** phase map, and **c** Al matrix boundary map
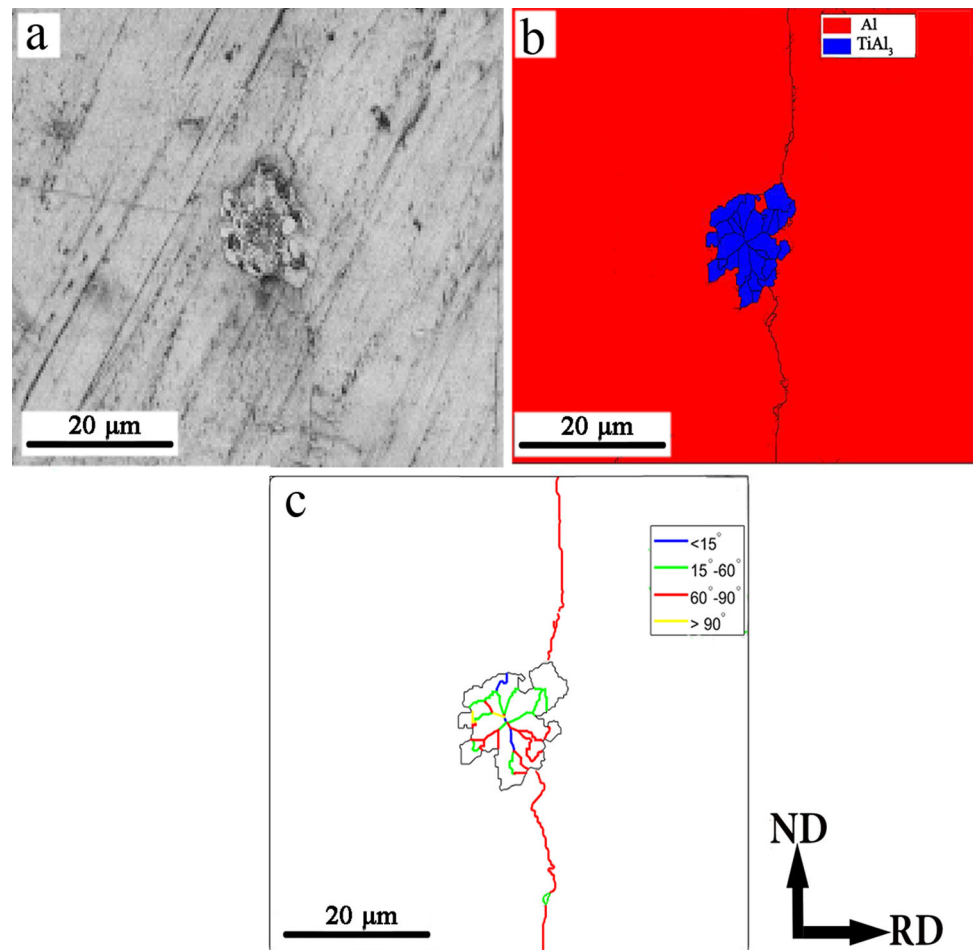
formation of the intermetallic compound at the final step of the process, the Kirkendall pores created are not eliminated, which reduces the strength, ductility, and density of the composite.

3.1.3 XRD Evaluations of CRB-AT-ARB and CRB-ARB-AT Composites

As already mentioned, the dislocation densities were calculated using the XRD patterns of different samples. Figure 7 demonstrates the XRD patterns of initial Al, CRB, CRB-AT, CRB-AT-ARB5, and CRB-ARB5-AT samples. It can be observed that after the CRB process, the XRD pattern shows peaks corresponding to only the Al matrix and the added Ti particles, but after the CRB-AT, almost all Ti is turned into the $TiAl_3$ phase. In XRD patterns, the crystallite size reduction and increasing internal stresses are considered by the diffraction peak broadening. The peak broadening value for the CRB-AT-ARB5 sample is higher than that for the CRB-ARB5-AT sample with a dislocation density of 45×10^{13} m^{-2} and 0.8×10^{13} m^{-2}, respectively. It can be reported that the grain refinement of

the ARB samples by increasing the number of ARB cycles is because of the formation of the boundaries with different geometries which are arranged in parallel bundles and according to the axis of the deformation [28]. In addition, there is a shift of Al peaks toward lower diffraction angles for cold rolled samples and also toward higher diffraction angles for heat treated samples. These changes could be due to high dislocation density and internal stresses in the first group, and low lattice size for the second group.

4 EBSD Evaluations in CRB-AT-ARB, Al-ARB, and CRB-ARB-AT Samples

4.1 CRB-AT-ARB Composite

The results of the EBSD analysis of the cold roll bonded and then annealed sample are presented in Fig. 8. The electron image in Fig. 8a shows the presence of a powder particle in the background of Al at the interface of the two layers. The associated phase analysis (Fig. 8b) illustrates that the powder particle has a chemical composition of the

Fig. 9 Diagram of the misorientation angle distribution of the **a** Al matrix and **b** TiAl₃ intermetallic compound in the CRB-AT sample
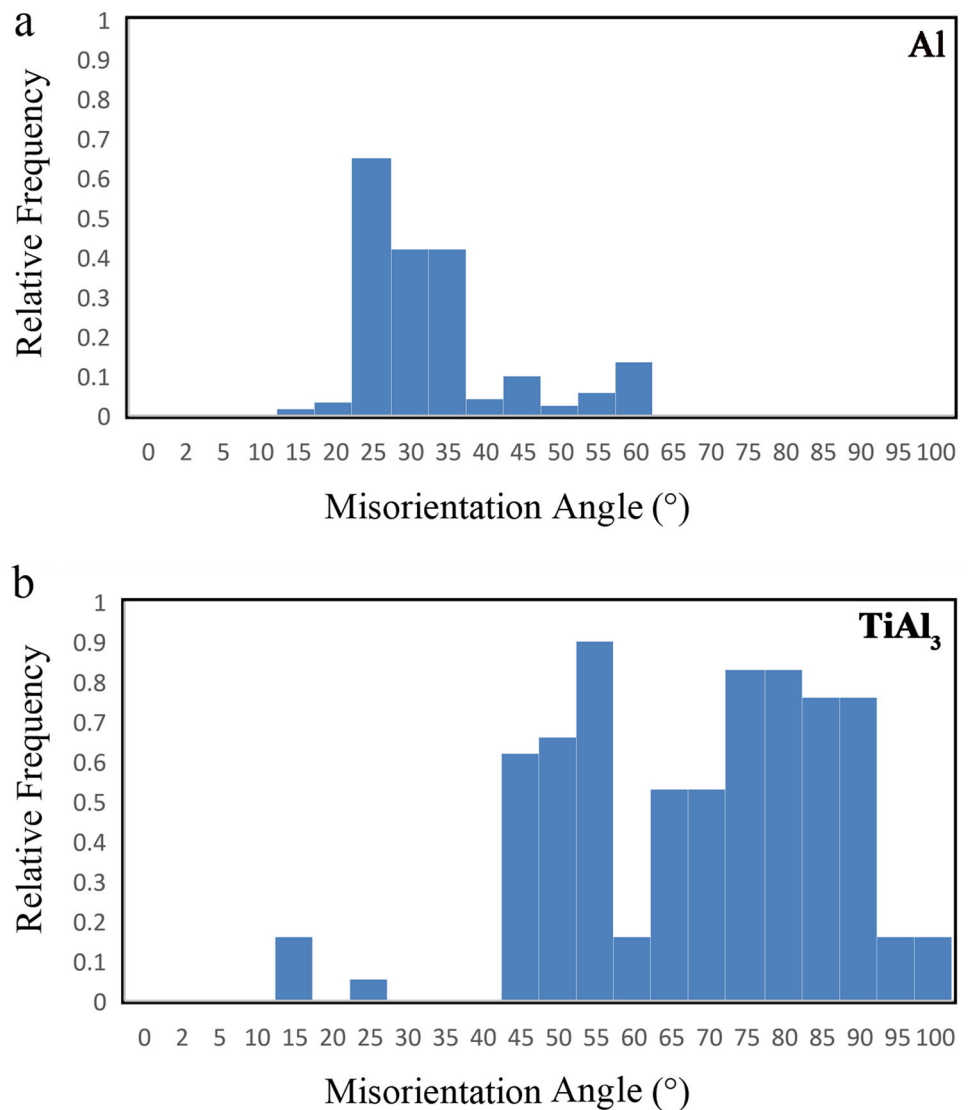

TiAl₃ intermetallic compound, marked in blue and placed on a red background in Al. The boundary map shown in Fig. 8c shows the main and secondary boundaries of the Al matrix with the misorientation angles. Thus, the main boundaries or high angles include misorientation angles of greater than 15°, and the sub-boundaries or low angles include misorientation angles of less than 15°. However, tiny low-angle boundaries containing misorientations of less than 2° have not been investigated due to the low accuracy of EBSD measurements [29]. According to this image, the boundaries formed in the matrix are the main boundaries with misorientation angles of greater than 15°. The grain size of Al after annealing at 590 °C for 2 h has become so large (about 60 μm) that, in this image, a complete Al grain is not seen, and there is a limited number of main grain boundaries between 2 Al grains.

Furthermore, the TiAl₃ intermetallic compound is a polycrystalline compound containing small grains. The average grain size for this compound is equal to 5 μm.

Figure 9 presents the misorientation angles distribution diagram obtained from the CRB-AT sample. Sections a and b of Fig. 9 show the distribution of the misorientation angles in the Al matrix and the TiAl₃ intermetallic compound in this sample, respectively. According to this figure, all existing boundaries belonging to both the matrix and the reinforcement particles are high-angle boundaries. The maximum intensity belongs to the misorientation angle of about 28° for the main Al boundaries.

The results of the EBSD inspection of the sample that underwent CRB, annealing, and then, five cycles of ARB (CRB-AT-ARB5) are presented in Fig. 10. The electron image in Fig. 10a shows the structure of fine-grained Al.

Fig. 10 Images obtained from the EBSD analysis of the CRB-AT-ARB5 sample in the ND-RD section, including **a** electron image, **b** phase map, and **c** Al matrix boundary map
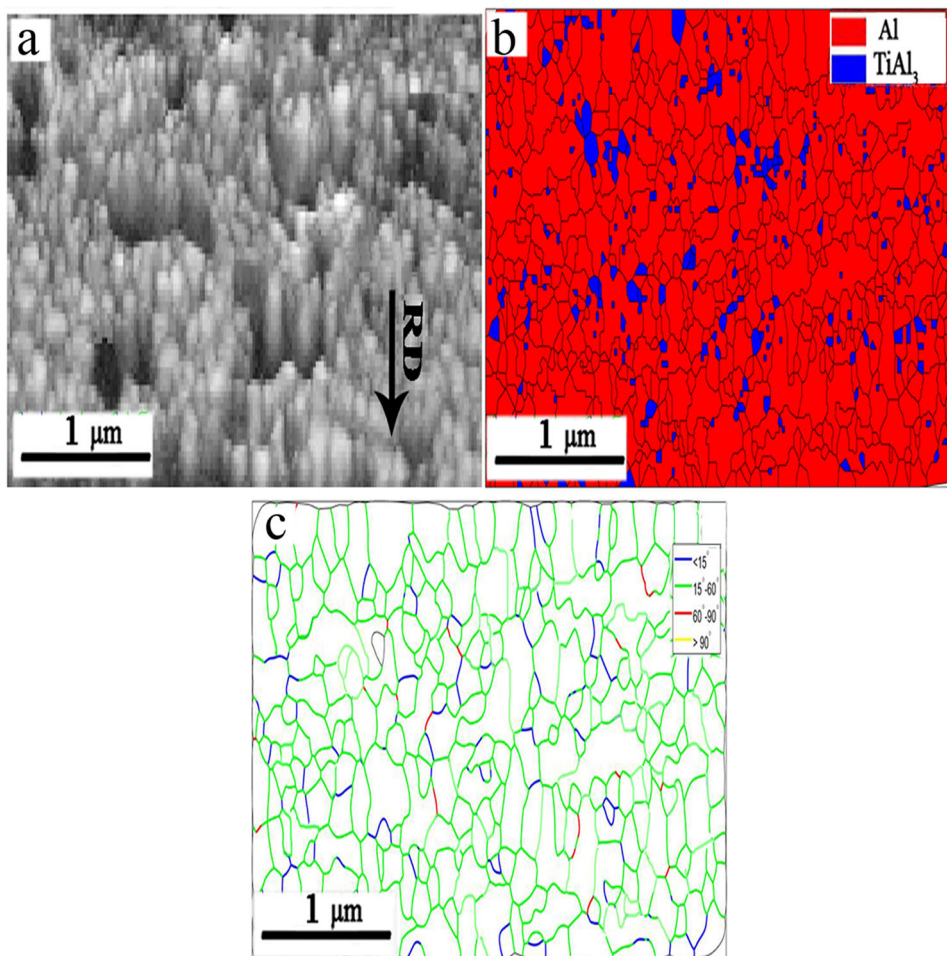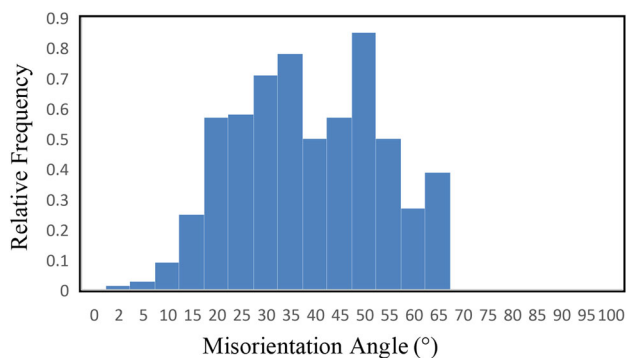

Fig. 11 Diagram of the misorientation angle distribution of the Al matrix in the CRB-AT-ARB5 sample
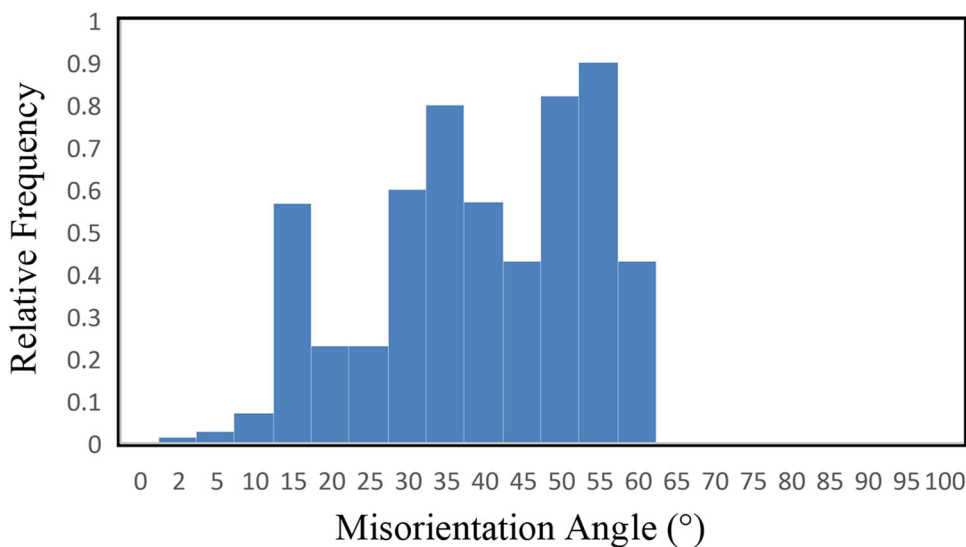
The maximum Al grain size is 500 nm. The elongation of the grains in the direction of rolling can also be seen. The associated phase analysis (Fig. 10b) illustrates that the $TiAl_3$ intermetallic compound marked in blue is uniformly distributed on the red Al matrix. The particle sizes of the intermetallic compound are within the nanometer range. The boundary map shown in Fig. 10c also indicates that these Al ultra-fine grains mainly have high-angle

Fig. 12 Images of the EBSD analysis of the Al-ARB5 sample in ND-RD section including **a** electron image, **b** phase map, and **c** Al boundary map

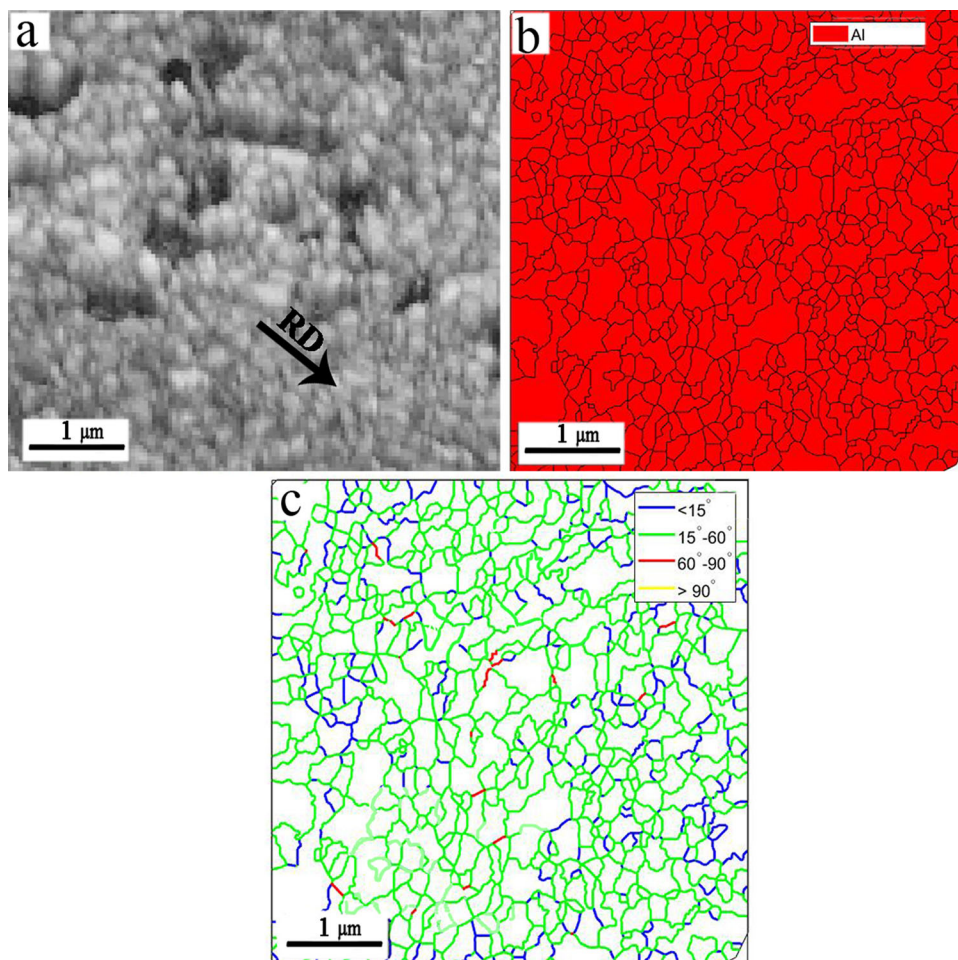**Fig. 13** Diagram of misorientation angle distribution in the Al-ARB5 sample

boundaries. Fine-grain formation occurs during severe plastic deformation as a result of the production and arrangement of dislocations in regular structures divided by high angular boundaries. The ARB sample shows that the lamellar structure is extended in the rolling direction. There are two kinds of boundaries in this structure, the lamellar boundaries (LBs) which are parallel to the rolling direction, and the short interconnecting boundaries (IBs) which

separate the layer boundaries vertically. The average distance between the lamellar boundaries in this sample is about 200 nm.

All materials that have undergone the ARB process contain large low-angle grain boundaries, but the contribution of high-angle boundaries is an essential factor for fine-grained severe plastic deformed structures [30]. The diagram of the misorientation angles distribution of the Al matrix related to this specimen is shown in Fig. 11. In this figure, it is observed that about 90% of the formed grain boundaries have high angles. Increasing the density of dislocations increases the mean intra-grain misorientation by increasing the strain [31]. The share of the main grain boundary increases in comparison with the Al sample before the ARB process. The misorientation of the main boundary with the maximum intensity also increases with increasing strain and reaches 55°.

4.2 Al-ARB Sample

The results of EBSD analysis of the 1100 Al sample without reinforcement particles, which underwent initial

Fig. 14 Images of the EBSD analysis of the CRB-ARB1-AT sample in the ND-RD section including **a** electron image, **b** phase map, and **c** Al matrix boundary map
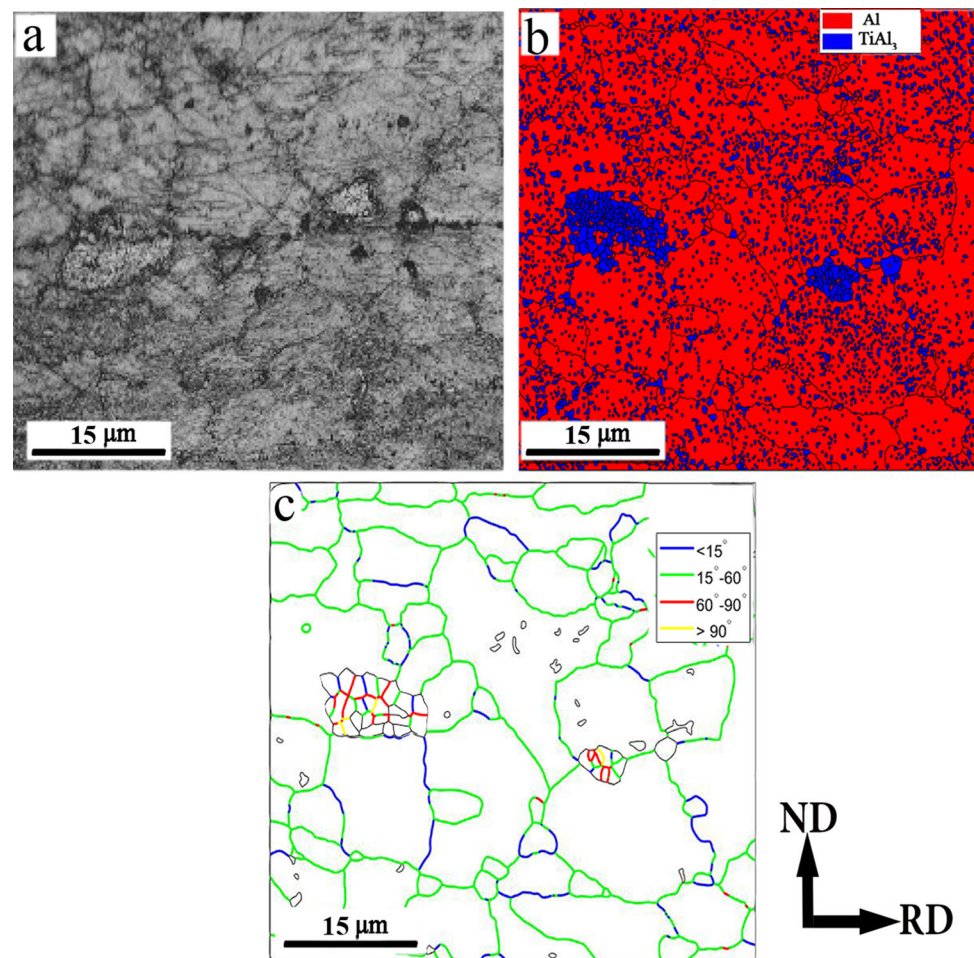
CRB, annealing, and then, five cycles of ARB (Al-ARB5) are illustrated in Fig. 12. The electron image in Fig. 12a shows that the Al structure with ultra-fine grains elongate in the rolling direction. The maximum grain size of Al is 700 nm. The associated phase analysis (Fig. 12b) shows that the red matrix belongs to Al. The boundary map in Fig. 12c also shows that these Al ultra-fine grains mainly have high-angle boundaries.

The diagram of the distribution of misorientation angles associated with this sample is shown in Fig. 13. As can be seen, about 80% of the formed grain boundaries have high angles. The share of high-angle boundaries has increased with ARB cycles. In this sample, the maximum distribution of the misorientation angle is about 50°. Observation of the lamellar structure has been reported by researchers in 1100 Al alloy, oxygen-free high thermal conductivity (OFHC) copper, and very low carbon steel after the ARB process with maximum strains of 3.2, 4.8, and 5.6, respectively [32, 33]. At low-to-medium strains, necessary geometric boundaries and inter-grain incidental dislocation boundaries are formed. The misorientation angles between these two types of boundaries also increase with increasing

strain, which leads to grain fracture into cells [34]. In Figs. 10 and 12, it can be seen that after five cycles of ARB, equiaxed grains are formed with an increase in ARB cycles. The formation of equiaxed grains in the fifth cycle confirms the occurrence of recrystallization in Al. The mechanism of the formation of ultra-fine grains during severe plastic deformation is still debated. A previous research on the EBSD of 1100 Al subjected to the ARB process showed that the ARB process resulted in a reduction in grain size, orientation in the rolling direction, and development of sub-grains and their conversion to main boundaries through dynamic recrystallization [35]. However, recent research [32] shows that the procedure of ultra-fine grains formation is not discontinuous, but is characterized by continuous recrystallization (including separation of very fine grains due to short-range grain boundary migration). Discontinuous recrystallization is believed to occur in materials with large initial grain size and low strain. In materials with smaller initial grain size and high strain, a microstructure with high-angle grain boundaries is formed through partial grain boundary movements with a continuous crystallization process [36]. It can be observed
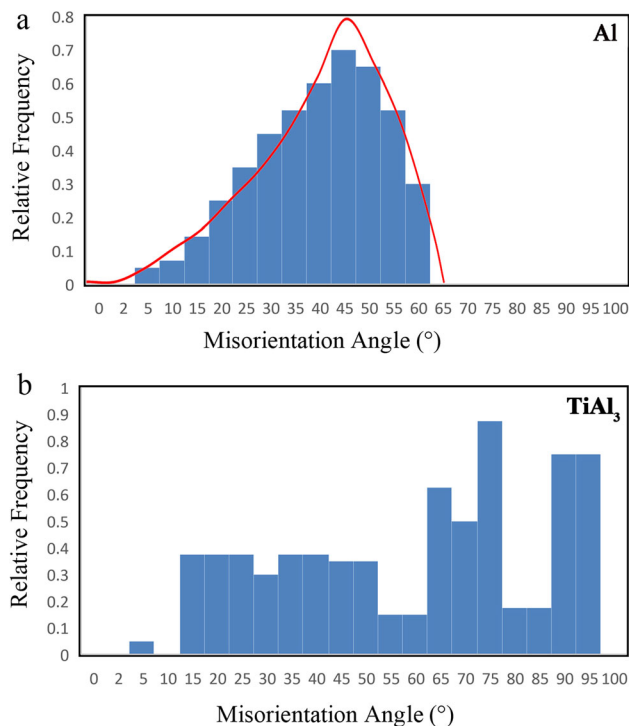
Fig. 15 Diagram of the misorientation angle distribution of **a** Al matrix (along with random texture distribution diagram in cubic structures) and **b** $TiAl_3$ intermetallic compounds in the CRB-ARB1-AT sample

that the presence of $TiAl_3$ intermetallic compound particles in the CRB-AT-ARB5 sample increases the mean misorientation angles compared to the Al sample without reinforcement particles (Al-ARB5). This difference is due to the presence of more strain in the Al layers in the composite sample than in the reinforcement particles. Al acts as a fluid base to accommodate the breakage of intermetallic particles during severe plastic deformation. Al matrix layers are softer, undergo more local deformation, and have more strain. Therefore, more grain refining occurs in this composite sample with greater grain size reduction [37].

4.3 CRB-ARB-AT Composite

The results of the EBSD analysis of samples after CRB and one cycle of ARB (with a strain of 0.8) and then annealing are demonstrated in Fig. 14. The electron image in Fig. 14a indicates the presence of $TiAl_3$ particles at the interface of the two Al layers. The associated phase analysis (Fig. 14b) indicates that these particles have the $TiAl_3$ intermetallic compound composition marked in blue color and placed on a red Al matrix. Grains as big as 30 μm are present in the Al matrix. The maximum particle size of the intermetallic compound is about 15 μm. The microstructure shows that the recovery, recrystallization, and grain growth phenomena have occurred due to annealing. It should be pointed

out that the recrystallization temperature for 1100 Al alloy is equal to 340 °C [37]. Therefore, recrystallization and grain growth at 590 °C can be expected. However, in the interface layer, non-uniform growth in Al grains is observed throughout the microstructure. This abnormal growth can be assigned to the existence of more strain in the interface and the presence of reinforcement particles in the intermetallic compounds. These factors make the grains that are located in the area around the $TiAl_3$ particles, act as a small deformation and elongate slightly in the rolling direction. There is a decrease in this abnormal growth due to annealing. The boundary map shown in Fig. 14c also shows that low-angle sub-grains are present within the high-angle Al grains.

The misorientation distribution diagram for the CRB-ARB1-AT sample is shown in Fig. 11. According to this figure, the Al matrix has a maximum intensity at a misorientation angle of 45° (Fig. 15a). Moreover, the distribution of misorientation angles in this sample is very close to the curve obtained for the random texture of cubic materials reported by Mackenzie [38]. According to Fig. 15b, the boundaries of the $TiAl_3$ intermetallic compound formed are almost all main boundaries and have high misorientation angles (average 75°).

The results of the EBSD analysis of the sample after CRB and five cycles of ARB (with a strain of 4) and then annealing are displayed in Fig. 16. The electron image in Fig. 16a illustrates the formation of a fine-grained structure next to bulky grains and the presence of small grains created through discontinuous static recrystallization during annealing. It also shows that the grains have entered the growth stage due to annealing. The associated phase analysis (Fig. 16b) indicates that the small particles marked in blue, placed in the red Al matrix, have the $TiAl_3$ intermetallic composition. The map of the Al boundaries in Fig. 16c shows that the recrystallized structure has main grain boundaries and the share of sub-grain boundaries in this sample is very small. This image shows a chain of small grains of at least 1 μ next to large grains with a maximum size of 20 μm. Nucleation of new grains during annealing alongside the rolling direction shows that there is an orientation-dependent recrystallization mechanism in this composite [39].

The misorientation distribution diagram of this sample and the Mackenzie random texture curve [38] is presented in Fig. 17. This diagram shows that almost all the main grains formed in this sample have a misorientation angle of higher than 15°, and the maximum misorientation is related to an angle of 50°. As mentioned, increasing strain before annealing leads to an increase in misorientation. Moreover, severe plastic deformation can cause a large number of misorientations within the material. These defects are the pathway for high-speed diffusion; therefore, diffusion into

Fig. 16 The EBSD analysis results of the CRB-ARB5-AT sample in the ND-RD section, including **a** electron image along with the ultra-fine grains structure, **b** phase map, and **c** Al matrix boundary map
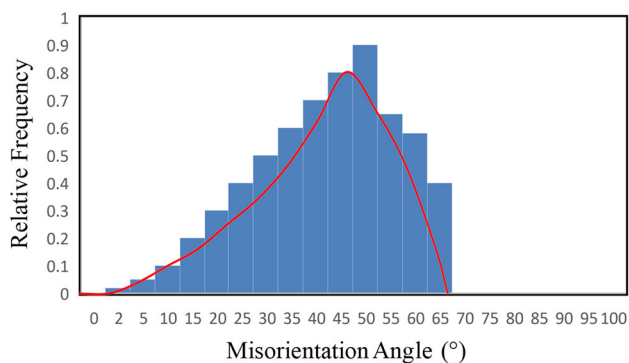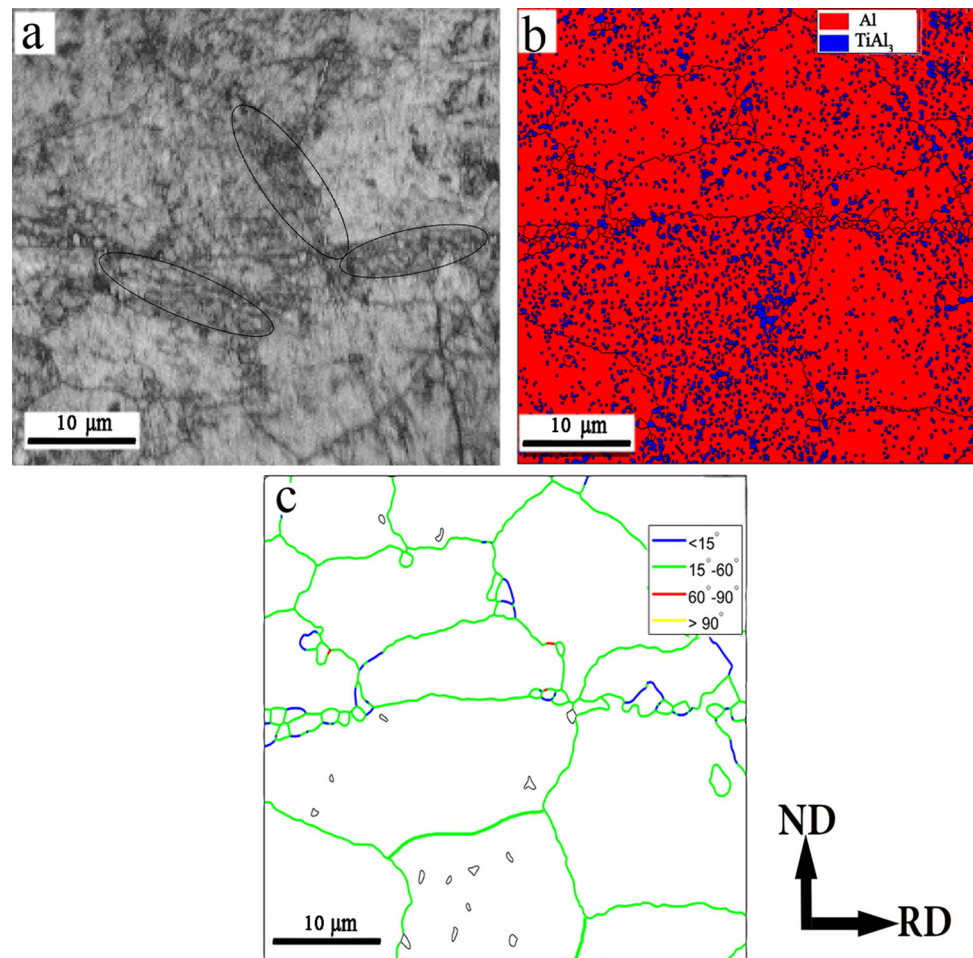
Fig. 17 Diagram of the misorientation angle distribution of the aluminum matrix in the CRB-ARB5-AT sample with random texture distribution diagram in cubic structures

fine-grained materials is much faster than coarse-grained materials. This will cause the elimination of dislocations during annealing and lead to a greater recovery process [40]. Therefore, according to Fig. 15, in this sample, the proportion of sub-grain boundaries is much less than that of the sample that underwent CRB, one cycle of ARB, and then, annealing. Furthermore, due to the reduction in size

and greater uniform distribution of reinforcement particles with growing strain, the average grain size in this sample is less than the CRB-ARB-AT sample (Fig. 14). Another point is the low misorientation angle of the CRB-ARB5-AT sample compared to the CRB-AT-ARB5 sample (Fig. 11), due to increasing grain size and reduction in strain.

5 Evaluations of Al Grain Size in CRB-AT-ARB, Al-ARB, and CRB-ARB-AT SAMPLES

5.1 CRB-AT-ARB Composite and Al-ARB Sample

The results of grain size calculations according to EBSD analysis are given in Table 1. In CRB-AT-ARB samples, after CRB and annealing, the main grain size of Al decreases with an increase in ARB cycles. The particle size of the intermetallic compound also decreases during ARB. According to Fig. 10c, the grain size of the Al matrix reaches about 500 nm after five ARB cycles, while it is about 700 nm for Ti-free Al under the same manufacturing

Table 1 Results of measuring the average grain size of CRB-AT-ARB and Al-ARB samples using EBSD analysis

Sample	Al matrix grain size (μm)	TiAl$_3$ particles size (μm)
Initial Al	≤ 20	–
CRB	≤ 3	–
CRB-AT	≤ 60	≤ 100
CRB-AT-ARB 1	1–5	0.7–40
CRB-AT-ARB 2	0.8–1	0.6–10
CRB-AT-ARB 3	0.5–0.8	0.5–10
CRB-AT-ARB 4	0.4–0.6	0.5–8
CRB-AT-ARB 5	0.2–0.5	0.2–5
Al-ARB 5	0.4–0.7	–

Table 2 Results of measuring the average grain size of CRB-ARB-AT samples using EBSD analysis

Sample	Al matrix grain size (μm)	TiAl$_3$ particles size (μm)
Initial Al	≤ 20	–
CRB	≤ 3	–
CRB-ARB1-AT	1–30	0.5–70
CRB-ARB3-AT	1–25	0.3–60
CRB-ARB5-AT	1–20	0.2–50

conditions. This difference indicates a decline in grain size caused by the presence of intermetallic compound particles [41].

Several factors contribute to the fine-graining of Al throughout the ARB procedure. One of these is severe shear deformation. This severe plastic deformation as a result of friction between the sheet and the roller under non-lubricating conditions leads to fine-graining with increase in the equivalent strain. This deformation region is transferred to the middle area of the sample with increase in ARB cycles, and therefore, the whole sample undergoes severe plastic deformation [42]. Another effective mechanism is continuous dynamic recrystallization in which nanoparticles and ultra-fine grains are generated in severe plastic deformed metals. With the formation of ultra-fine grains, the creation of boundaries is accompanied by a recovery process and short-range grain boundary migration.

The occurrence of continuous dynamic recrystallization during rolling in Al has been reported by other researchers [6, 15, 43, 44]. Tsuji et al. [8] also described the grain refining mechanism in the ARB method as grain fragmentation. In this mechanism, the primary coarse grains are divided into several smaller grains due to plastic deformation. In the initial cycles, a significant number of dislocations are formed in the structure, and with the enhancing number of cycles, the density of dislocations increases and they form sub-grains. The grains formed at this stage have low-angle boundaries. In the latter stages of the ARB process, low-angle boundaries become high-angle boundaries, resulting in ultra-fine grains throughout the structure.

The most important effects of particles on continuous recrystallization and thus reducing the grain size of the composite are, first, the existence of particles and stored energy, and consequently, increase in the driving force of continuous recrystallization, and second, the behavior of large particles as continuous recrystallization nucleation locations. Moreover, fine reinforcement particles with uniform distribution in the structure can be a factor for fine refining. These particles are barriers to the movement of dislocations and cause the accumulation of dislocations and the formation of sub-grains. This high density of dislocations leads to stress concentration and higher grain boundary diffusion and thus accelerates boundary formation due to the presence of more misorientation. In general, during the ARB process, a set of mechanisms occurs in Al, and after five ARB cycles, a fine-grained structure is obtained. The occurrence of these mechanisms has been confirmed by other researchers [7, 42].

A noteworthy finding is the breaking up of the intermetallic composition of TiAl$_3$ during the rolling process and the achievement of a uniform distribution of particles along with a further reduction in grain size due to the presence of particles.
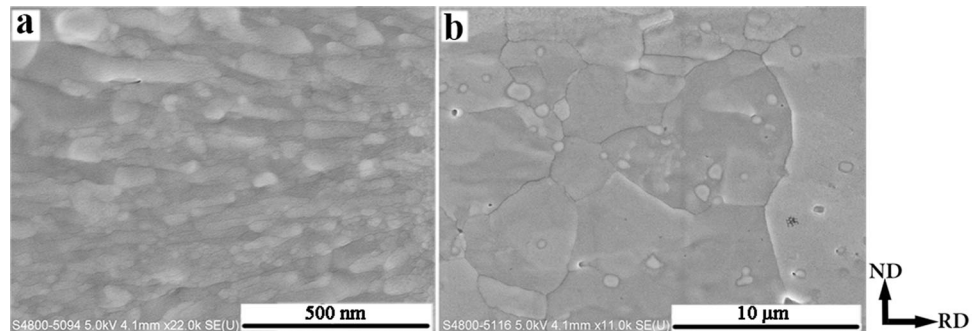
5.2 CRB-ARB-AT Composite

The results of measuring the grain size of Al and intermetallic compound particles through the EBSD analysis are given in Table 2. It can be seen that due to the ARB process, Al grain size has reached a small 1 μm, and the minimum particle size of the intermetallic compound has been reduced to 200 nm. Due to factors such as surface preparation of the sheets and lack of lubrication, the shear strain component is large and will perform an essential function in the development of ultra-fine grains [37]. Through comparison with the results presented in Table 1, it can be concluded that annealing has caused the grains to grow. In addition, the particle size of the intermetallic compound has a wide range. As mentioned, the presence of

Fig. 18 Optical microscope images of **a** CRB-AT-ARB5 and **b** CRB-ARB5-AT samples
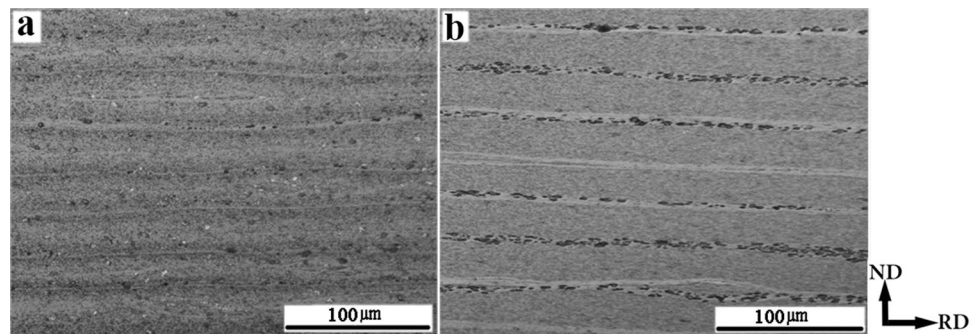
Fig. 19 Field emission scanning electron microscope images of **a** CRB-AT-ARB5 and **b** CRB-ARB5-AT samples

large-sized $TiAl_3$ intermetallic particles is due to the insufficient fineness of Ti powders during the five cycles of ARB.

6 Comparison of CRB-AT-ARB and CRB-ARB-AT Composite Samples

In this section, the effects of annealing before and after ARB on microstructural characteristics are briefly investigated. An overview of the final Al-$TiAl_3$ samples obtained using optical microscope images is presented in Fig. 18. In Fig. 18a, an image of a CRB-AT-ARB5 sample is presented. According to this image, the final structure is in the form of a compact layer containing a fine-grained Al matrix with a suitable distribution of $TiAl_3$ intermetallic compound particles. The optical microscope image of the CRB-ARB5-AT sample is shown in Fig. 18b. This image shows the lamellar structure in this sample. This figure reveals the presence of a recrystallized Al matrix placed between the particles of the $TiAl_3$ intermetallic compound at the site of the interface. Reinforcement particles are mainly present in the interface and, therefore, have a less uniform distribution than in Fig. 18a.

A comparison of these two samples at further magnification has also been performed using FESEM. FESEM images obtained from the CRB-AT-ARB5 and CRB-ARB5-AT samples are presented in Figs. 19a and b, respectively. Evaluations of these images confirm that performing 1–5 cycles of ARB after annealing (Fig. 19a)

lead to the expansion of the stretched lamellar structure with a thickness of a few nanometers in the rolling direction in the Al matrix, but performing annealing after ARB (Fig. 19b) results in the formation of a dual recrystallized structure of Al with large grains of 30 μm alongside smaller grains. It is discovered that, in the ARB process, increasing the density of dislocations is one of the main mechanisms of grain refining, while in the case of annealing after rolling, it is recrystallization. This is in line with previous reports by Zhang et al. and Zhao et al. [45, 46].

7 Conclusions

In the present study, using EBSD analysis, a microstructural evaluation was performed on Al matrix composites with $TiAl_3$ reinforcement particles made through various ARB and annealing methods on 1100 Al sheets and pure Ti powders. The main results of this article are as follows:

1. CRB and then annealing of Al sheet/Ti powder/Al sheet layers led to the formation of $TiAl_3$ intermetallic compound particles in the Al matrix.
2. Performing 1–5 cycles of ARB after annealing led to the fabrication of an ultra-fine Al composite with a size of about 500 nm containing a uniform distribution of $TiAl_3$ intermetallic compound particles with dimensions larger than 200 nm. The grain size of Al in the

sample of non-reinforcing aluminum particles made under the same conditions was about 700 nm.

3. The presence of reinforcement particles led to increasing the density of dislocations and providing suitable places for the nucleation of sub-grains in the Al matrix and consequently, the larger grain refinement of the matrix was possible.

4. The average misorientation angle and volume fraction of high-angle grain boundaries increased with the increasing number of ARB cycles.

5. The microstructure evaluation of the composite made through the CRB-ARB-AT method showed that the Al grain size obtained after ARB and annealing processes was in micrometer and extensive, and the intermetallic compound consisted of a wide range of particle sizes, between 0.2 μm and 50 μm.

6. In the CRB-ARB-AT samples, with increasing ARB cycles, both the volume fraction of high-angle grain boundaries after annealing and the average misorientation angle increased. In comparison, the share of low-angle grain boundaries decreased due to a more significant recovery process.

7. Annealing before the ARB process caused the formation of a compact layer with a reduced number of voids, while annealing after the ARB process increased the number of voids and created an equiaxed structure.

8. The strength of the composite produced using CRB–annealing–ARB process increased with ARB cycles and, in the end, reached 400 MPa. The strengthening of the Al-TiAl$_3$ composite was essentially due to reduction in the grain size of Al and the presence of TiAl$_3$ intermetallic particles.

9. A compact layered structure with little porosity, and high strength and hardness was developed due to annealing before the ARB process, while annealing after the ARB process resulted in increased porosity, decreased strength, and hardness, and a uniaxial grain structure.

References

[1] Rana R S, Purohit R, and Das S, Int. J. Eng. Res. **3** (2012) 1-16.
[2] Clyne T W, in *Metal matrix composites: Matrices and processing*, (ed) Mortensen A, Elsevier, 2001.
[3] Heathcote J, Odette G, Lucas G, Rowe R, and Skelly D, Acta Mater. **44** (1996) 2489.
[4] Lesuer D, and Syn. C, in *Metallic laminates for engine applications*, 8th CIMTEC World Ceramics Congress & Forum on New Materials, Italy, (1994).
[5] Massalski T, *binary alloy phase diagrams*, American society for metals, (1986).
[6] Saito Y, Tsuji N, Utsunomiya H, Sakai T, and Hong R G, Scr. Mater. **39** (1998) 1221–1227.
[7] Saito Y, Utsunomiya H, Tsuji N, and Sakai T, Acta Mater. **47** (1999) 579–583.
[8] Tsuji N, Ito Y, Saito Y, and Minamino Y, Scr. Mater. **47** (2002) 893-899.
[9] Oh J, Pyo S G, Lee S, and Kim N J, J. Mater. Sci. **38** (2003) 3647 – 3651.
[10] Luo J G, and Acoff V L, Mater. Sci. Eng. A **379** (2004) 164–172.
[11] Chaudhari G P, Acoff V L, Intermetallics **18** (2010) 472–478.
[12] Sieber H, and Perepezko J H, in *Intermetallic Phase Formation in Bulk Multilayered Structures*, (Eds.) Morris D G, Naka S, and Caron P, WILEY-VCH Verlag GmbH, Weinheim. (2000) pp. 324–329.
[13] Yang D K, Hodgson P, and Cui E W, Intermetallics **17** (2009) 727–732.
[14] Liu C Y, Jing R, Wang Q, Zhang B, Jia Y Z, Ma M Z, and Liu R P, Mater. Sci. Eng. A **558** (2012) 510-516.
[15] Yazdani Z, Toroghinejad M R, Edris H, and Ngan A H W, J. Alloys Compd. **747** (2018) 217-226.
[16] Loo F V, and Rieck G, Acta Metall. Mater. **21** (1973) 61-71.
[17] Yazdani Z, Toroghinejad M R, Edris H, and Ngan A H W, Trans. Indian Inst. Met. **71** (2018) 2497–2504.
[18] Azushima A, Kopp R, Korhonen A, Yang D Y, Micari F, Lahoti G D, Groche P, Yanagimoto J, Tsuji N, Rosochowski A, and Yanagida A, CIRP Ann Manuf Technol **57** (2008) 716–735.
[19] Smallman R E, and Westmacott K H, Philos. Mag. **2** (1957) 669-683.
[20] Loo F V, and Rieck G, Acta Metall. Mater. **21** (1973) 73.
[21] Xu L, Cui Y, Hao Y L, and Yang R, Mater. Sci. Eng. A **435–436** (2006) 638–647.
[22] Chianeh V A, Hosseini H M, and Nofar M, J. Alloys Compd. **473** (2009) 127-132.
[23] Jamaati R, and Toroghinejad M R, Mater. Des. **31** (2010) 4816–4822.
[24] Guan R, and Tie D, Acta Metall. Sin. (Engl. Lett.) **30** (2017) 409-432.
[25] Lin H R, Tian Y Z, and Sun S J, Acta Metall. Sin. (Engl. Lett.) **34** (2021) 925–931.
[26] Muhammad W, Brahme A P, Sabat R K, Mishra R K, and Inal K, Mater. Sci. Eng. A **759** (2019) 613–623.
[27] Fukutomi H, Nakamura M, Suzuki T, Takagi S, and Kikuchi S, Mater. Trans. **41** (2000) 1244.
[28] Rahmatabadi D, Hashemi R, Mohammadi B, and Shojaee T, Mater. Sci. Eng. A **708** (2017) 301–310.
[29] Tsuji N, Ueji R, and Minamino Y, Scr. Mater. **47** (2002) 69-76.
[30] Kim H W, Kang S B, Tsuji N, and Minamino Y, Metall. Mater. Trans. A **36** (2005) 3151–3163
[31] [31] Li Z G, Li N, Jiang H W, Xiong Y, and Liu L, J. Alloys Compd. **589** (2014) 164–173.
[32] Tesuji N, Lee Y, and Minamino Y, Adv. Eng. Mater. **5** (2003) 338-344.
[33] Tsuji N, Minamino Y, and Hansen N, in *Science of metastable and nanocrystalline alloys. Structure, properties and modelling*, (edn) Dinesen A.R., Eldrup M, Jensen D J, Linderoth S, Pedersen T B, Pryds N H, Pedersen A S, and Wert J A, Proceedings, Roskilde (2001) pp. 255–262.
[34] Bay B, Hansen N, Hughes D A, and Kuhlmann-Wilsdorf D, Acta Metall. Mater. **40** (1992) 205-219.
[35] Jaehyung C, Hyung-Wook K, and Cha-Yong L, *Texture and Microstructure Evolution of AA1100 during Accumulative Roll Bonding*, Proceedings of the 12th International Conference on Aluminium Alloys, Yokohama, Japan (2010) pp. 143–148.
[36] Humphreys F J, and Hatherly M, *Recrystallization and related annealing phenomena*, Elsevier, Oxford (2004).
[37] Yang D K, Cizek P, Hodgson P, and Cui E W, Scr. Mater. **62** (2010) 321–324.
[38] Mackenzie J K, Acta Metall. Mater. **12** (1964) 223-225.

[39] Sabat R K, Sahoo S K, Panda D, Mohanty U K, and Suwas S, Mater. Charact.**132** (2017) 388–396.

[40] Takata N, Yamada K, Ikeda K, Yoshida F, Nakashima H, Tsuji N, Mater. Trans.**48** (2007) 2043-2048.

[41] Singh P B, Sabat R K, Kumaran S, J. Mater. Eng. Perform**27** (2018).

[42] Jamaati R, Toroghinejad M R, Dutkiewicz J, Szpunar J A, Mater. Des.**35** (2012) 37–42.

[43] Ivanov K V, Structure, AIP Conf. Proc., (2016) pp. 20–76.

[44] Sabat R K, Pavan M V S S D S S, Aakash D S, Kumar M, Sahoo S K, Philos. Mag. (2018) 2562–2581.

[45] Zhang L, Wang Y, Yang X, Li K, Ni S, Du Y, and Song M, Mater. Res.**20** (2017) 1360-1368.

[46] Zhao Q, Liu Z, Huang T, Mater. Charact.**119** (2016) 47-54.

Publisher's Note Springer Nature remains neutral with regard to jurisdictional claims in published maps and institutional affiliations.